CENTRALITY DEPENDENCE OF BULK FIREBALL PROPERTIES IN $\sqrt{s_{NN}}$ = 62.4 and 200 GeV

By

WILLIAM CHESLUK PARKER

A Thesis Submitted to The Honors College

In Partial Fulfillment of the Bachelor's degree
With Honors in

Physics

THE UNIVERSITY OF ARIZONA

May 2009

Approved by:

_____

Dr. Johann Rafelski
Department of Physics

STATEMENT BY AUTHOR

I hereby grant to the University of Arizona Library the nonexclusive worldwide right to reproduce and distribute my thesis and abstract (herein, the “licensed materials”), in whole or in part, in any and all media of distribution and in any format in existence now or developed in the future. I represent and warrant to the University of Arizona that the licensed materials are my original work, that I am the sole owner of all rights in and to the licensed materials, and that none of the licensed materials infringe or violate the rights of others. I further represent that I have obtained all necessary rights to permit the University of Arizona Library to reproduce and distribute any nonpublic third party software necessary to access, display, run, or print my thesis. I acknowledge that University of Arizona Library may elect not to distribute my thesis in digital format if, in its reasonable judgment, it believes all such rights have not been secured.

SIGNED: _____

Ten microseconds after the big bang, the early universe was filled with a hot dense state of matter called the Quark-Gluon Plasma. Over time the universe expanded and matter cooled, eventually reaching its present state. Today in the laboratory we attempt to recreate this phase of matter. At the Relativistic Heavy Ion Collider (RHIC) at Brookhaven National Laboratory, nuclei are collided at speeds of up to 99.995% the speed of light to attempt to recreate conditions similar to the early universe, if only briefly.

For analysis of data from this experiment we use SHARE (Statistical Hadronization with Resonances), a program developed at the University of Arizona by Giorgio Torierri and Johann Rafelski to fit bulk physical properties to the experimentally measured RHIC particle yields. SHARE is an important tool for the study of relativistic heavy ion collisions, and a major component of my senior thesis has been developing proficiency with the program.

The product of this effort is an analysis of the highest energy data available today from RHIC, with center of mass energy of 200 GeV per nucleon. We expand upon previous studies to present a comprehensive analysis of the dependence of the bulk physical properties upon the centrality of the collisions. This analysis is done in parallel with University of Arizona graduate student Michal Petran. He is analyzing RHIC data at center of mass energy 62.4 GeV using a similar method. Together we have written the attached paper considering among other things the differences between relativistic heavy ion collisions at 62.4 and 200 GeV.

My contribution to the attached paper is the analysis, discussion, and presentation at 200 GeV. By including these results we are able to comment on the behavior of physical properties with respect to energy as well as centrality. The attached paper is a draft of the paper to be published. I will remain with the group after the completion of my thesis to see the paper through to publication.

Centrality dependence of bulk fireball properties in $\sqrt{s_{NN}} = 62.4$ GeV Au-Au collisions

Michal Petran[1],* William Parker[1], Jean Letessier[2], Giorgio Torrieri[3], and Johann Rafelski[1]

[1] *Department of Physics, University of Arizona, Tucson, Arizona 85721, USA*
[2] *Laboratoire de Physique Théorique et Hautes Energies, Université Paris 7, 2 place Jussieu, F-75251 Cedex 05, France and*
[3] *Frankfurt Institute of Advanced Studies, Johann Wolfgang Goethe Universität, Ruth-Moufang-Str. 1, 60438 Frankfurt am Main, Germany*

(Dated: May 4, 2009)

We present the centrality dependence of the bulk properties of a fireball created in $\sqrt{s_{NN}} = 62.4$ GeV and $\sqrt{s_{NN}} = 200$ GeV Au-Au collisions at the Relativistic Heavy–Ion Collider. First we explore the centrality dependence of particle yields. Then we fit particle yields with statistical hadronization model and present the resulting model parameters, rapidity yields of physical quantities and bulk properties. We show the behavior these quantities as a function of centrality and compare them for both available energies.

PACS numbers: 24.10.Pa, 13.60.Rj, 12.38.Mh, 25.75.-q

I. INTRODUCTION

The Relativistic Heavy Ion Collider (RHIC) makes possible the study of the physical properties of dense hadronic matter at the point of hadronization. In particular the experiment STAR provides useful data for particle yields at mid-rapidity. This article will focus on the centrality dependence of various bulk properties of the fireball created in a relativistic heavy ion collision.
We are working with the lower RHIC energy $\sqrt{s_{NN}} = 62.4$ GeV and the top $\sqrt{s_{NN}} = 200$ GeV energy Au-Au collisions, for which we have data from either STAR or PHENIX experiment in different centrality bins. In order to unify the centrality binning for different particle species, we present a fit to particle data across number of participants (N_{part}) (detailed description follows in section II). Specifically, we emphasize the successful fitting of recent data for ϕ [1] on the background of other (both strange and non-strange) particles [2],[3] at 62.4 GeV. Also, several hadronization conditions are discussed in the context of analysis done for SPS at lower energies and top RHIC energy $\sqrt{s_{NN}} = 200$ GeV.

II. DATA

A. Relative Particle Yields

At 200 GeV we observe enhanced pair production for the π^-, K^+, p^+ and associated anti-particles, relative to 62.4 GeV. However the Λ, Ξ^-, and Ω show no such enhancement. This shows that strangeness enhancement is not as pronounced at 200 GeV as it is at 62.4 GeV. The reasons for this are discussed further in Section IV. Only one particle does not follow this pattern, which is the ϕ. Based on the other particles, we would expect normalized ϕ abundance to be reduced at 200 GeV, but it is approximately the same as 62.4 GeV. Interestingly, when we fit the data, SHARE predicts a 200 GeV ϕ yield well below the experimental data (see subsection IV A for further discussion). With ϕ included the fit is significantly different, and so for 200 GeV we choose not to include it in our analysis.

B. 62.4 GeV

We have collected data from various sources [1–4]. We end up with data for $\pi^{\pm}$, $K^{\pm}$, $p^{\pm}$, $\Lambda, \overline{\Lambda}$, ϕ, $\Xi^{\mp}$, $\Omega^{\mp}$ expressed in 13 incompatible centrality bins. Therefore, we translate the centrality bins to number of participants of the collision (N_{part}) as seen (for example) in Table 1 in [7]. The data we have can be seen in bold in Table V. Then we fit every particle (and antiparticle) yield with the following function

$$g(x) = ax^b + c, \tag{1}$$

where a,b and c are free real parameters and x the variable, being in this case (and further in this work) the number of participants, and variables are defined as in Eq.1. We obtained very good fit on the range $N_{part} \in (50, 360)$. The respective confidence levels are shown in Table II. We show the result of our effort for particles and antiparticles in top and middle plot of Figure 2. Note that for further use we combine the Ωs yields together and use $(\Omega + \overline{\Omega})$ for further analysis. Then we use p^+/p^- and $\Lambda/\overline{\Lambda}$ ratios both fitted with (bottom plot in Fig. 2)

$$h(x) = 1 + a \tanh(b(x - c)). \tag{2}$$

Reasons for this effort are discussed further in this work in section IV.

*Electronic address: mpetran@email.arizona.edu

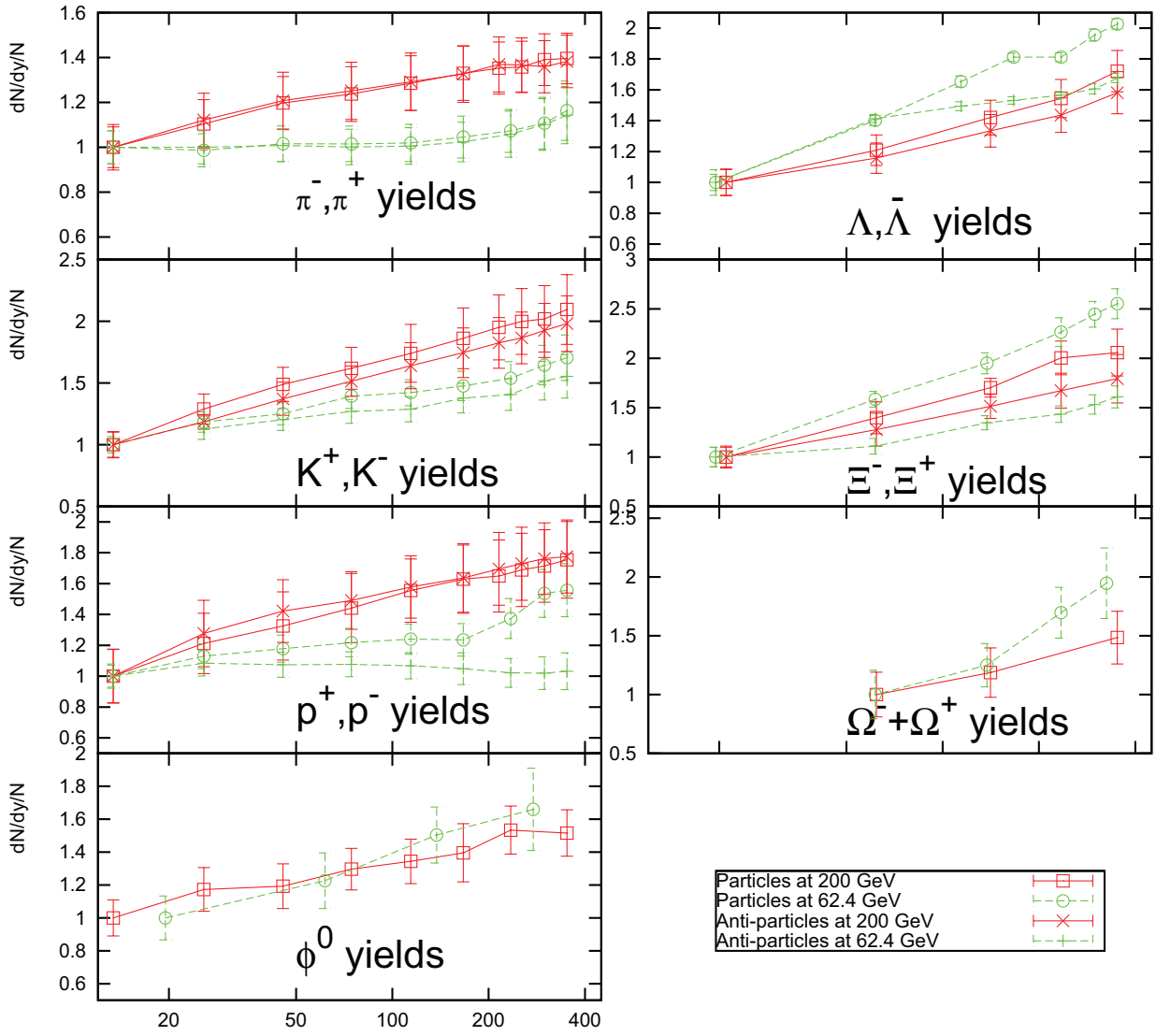

FIG. 1: Particle yields at 62.4 and 200 GeV, normalized to most peripheral data for each particle.

We introduce continuous functions for particle yield interpolation because we believe that doing so will make our physical fit much more compatible as in fact we are reducing the effect of statistical experimental error for every particle yield. Final parameter values can be seen in Table I together with the χ^2 of each fit and the associated statistical significance (also referred to as confidence level in some texts). This number can be understood as the probability that our function indeed describes the given datapoints. The reader can find detailed description and discussion in chapter 32.3.1 of [8]. Most of the particles rank very high in terms of statistical significance; the functions describes their behavior very accurately. Results slightly above 60% for ϕ and $(\Omega + \overline{\Omega})$ are still considered good since we were working with only one degree of freedom for each of them. The only fit that is at first sight incompatible is the Λ. We had newer data for Λ with much lower errors. This is evident from bottom plot of Fig.2. If one takes a close look at graphs in Fig.2, Λ and $\overline{\Lambda}$ are fitted as well as other particles. The differ-

TABLE I: Particle yields power fit parameters (as defined by Eq.1) used to determine particle yields, where no data was available. The used values can be seen in Table V.

$\sqrt{s_{NN}} = 62.4GeV$

	a	b	c
π^-	0.421	1.072	0.9891
π^+	0.475	1.048	0.2270
K^+	0.055	1.111	-0.1208
K^-	0.048	1.107	-0.0438
Λ	0.015	1.165	-0.1013
$\overline{\Lambda}$	0.015	1.051	-0.0925
Ξ^-	0.001	1.247	-0.0097
$\overline{\Xi}^+$	0.001	1.221	0.0009
$\Omega + \overline{\Omega}$	0.000085	1.437	0.000044
p^+	0.047	1.115	0.0150
p^-	0.055	0.941	-0.1209
ϕ^0	0.004	1.203	0.0013
p^+/p^-	22.844	0.00011	-257.8680
$\Lambda/\overline{\Lambda}$	0.962	0.004	-140.4570

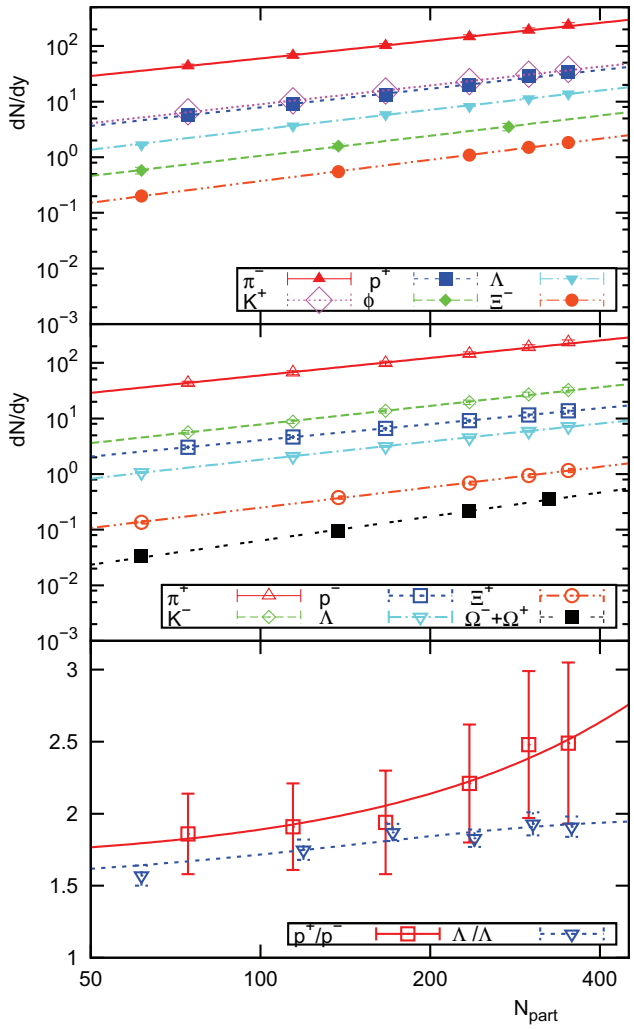

FIG. 2: Fit to particles' yields data at 62.4 GeV.

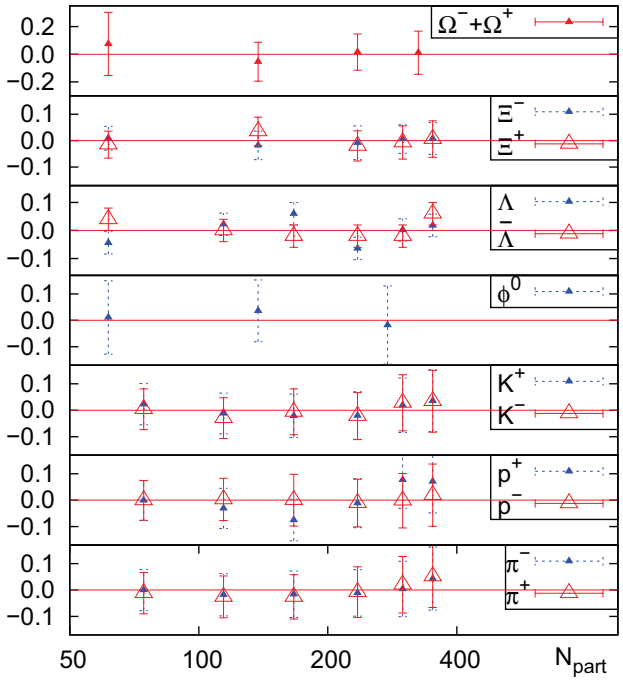

FIG. 3: The difference between experimental values and fitted function with errors all scaled with the theoretically predicted value $((data - fit)/fit \pm error/fit)$ at 62.4 GeV.

ences of particle yields and the fited functions are shown in Fig.3. Summary of actually used values can be found in Table V. The motivation to fit proton and Λ ratios is discussed further in Section III.

C. 200 GeV

We use data from the PHENIX collaboration [12] for $\pi^{\pm}$, $K^{\pm}$, $p^{\pm}$, and STAR data for $\Lambda, \overline{\Lambda}$, ϕ, $\Xi^{\mp}$, and $\Omega^- + \Omega^+$ [13, 14]. Because much of the data is in incompatible centrality bins we translate to number of participants (N_{part}) [7]. In order to interpolate between different N_{part} we fit particle and antiparticle yields with the power function

$$f(x) = ax^b + c \tag{3}$$

where x is the number of participants and a, b, and c are determined by the fit. The results of the interpolation can be seen in Table III. We determine the goodness

TABLE II: Particle yields fit quality expressed in χ^2 per degree of freedom and confidence level of particle yield interpolation (CL-I).

	200 GeV fit		62.4 GeV fit	
	χ^2/ndf	CL-I	χ^2/ndf	CL-I
π^-	0.025/6	99.99%	0.305/6	99.95%
π^+	0.240/6	99.97%	0.663/6	99.53%
K^+	0.033/6	99.99%	0.495/6	99.79%
K^-	0.152/6	99.99%	0.443/6	99.85%
Λ	0.813/2	93.68%	9.585/4	4.80%
$\overline{\Lambda}$	0.654/2	72.10%	4.480/4	34.49%
Ξ^-	1.612/2	44.67%	0.200/3	97.76%
$\overline{\Xi}^+$	0.194/2	90.76%	0.650/3	88.49%
$\Omega + \overline{\Omega}$	0.032/0	--	0.170/1	68.02%
p^+	0.033/6	99.99%	2.36/6	88.42%
p^-	0.033/6	99.99%	0.088/6	99.99%
ϕ^0	0.610/3	89.42%	0.129/1	71.99%
p^+/p^-	--	--	0.216/6	99.98%
$\Lambda/\overline{\Lambda}$	--	--	2.96/4	56.45%

of fit by χ^2 and confidence level, which can be found in Table II. As in the 62.4 GeV case we choose to use particle-antiparticle ratios for protons and Λs. However, rather than interpolating between different ratio values we interpolate between absolute yields, then use the ratio of the yields for our study. For all data with six degrees of freedom, we have a confidence level of over 99%. We are unable to achieve this for the particles with fewer degrees of freedom. As can be seen in Figure 5 despite

TABLE III: Particle yields power fit parameters (as defined by Eq.1) used to determine particle yields. The used values can be seen in Table V.

$\sqrt{s_{NN}} = 200GeV$

	a	b	c
π^-	0.671	1.034	-1.755
π^+	0.475	1.048	-1.132
K^+	0.060	1.143	-0.245
K^-	0.050	1.162	-0.152
Λ	0.011	1.244	0.085
$\overline{\Lambda}$	0.010	1.218	0.071
Ξ^-	0.003	1.131	-0.015
$\overline{\Xi}^+$	0.002	1.174	-0.008
$\Omega + \overline{\Omega}$	0.00032	1.265	0.0044
p^+	0.030	1.099	-0.122
p^-	0.022	1.093	-0.083
ϕ^0	0.019	1.035	-0.219

the low significance, the fitted values remain close to the experimental data.

In the upper two plots can be seen the results of our interpolation. For Λ and p^+ and their respective anti-particles, we use the ratio of particle to anti-particle yields rather than the yields themselves. In addition to rendering compatible different centrality bins interpolation allows us to study physical properties across centrality more continuously and reduces the statistical experimental error for each individual point.

III. STATISTICAL HADRONIZATION MODEL (SHM)

We used the statistical hadronization model implemented in the numerical package SHARE (Statistical Hadronization with Resonances, [10, 11]). Currently there are 3 possible statistical hadronization models, chemical non-equilibrium, semi-equilibrium and equilibrium (for details and discussion see for example [9]). Based on the data we have we could not distinguish between the three, but we are inclined to the non equilibrium. Furthermore, as discussed in [6], we introduce two hadronization conditions, which are critical pressure $P = 82\,\mathrm{MeV/fm^3}$ and energy per primary hadron $E/h_p = 750\,\mathrm{MeV}$. We introduce these two conditions as additional measured values together with strangeness conservation and net charge per net baryon conservation. Apart from the particle yields and ratios as introduced in section II, we constrain the system with 4 additional virtually measured values common for all centralities. The precise form of these constraints are presented in Table IV.

Our results were not consistent anymore for $N_{part} < 50$, therefore all results are shown for more than 50 participants. To test our particle yield fitting procedure, we fill the range with centrality bins, which use only our interpolated values, not a single real data point. It is shown

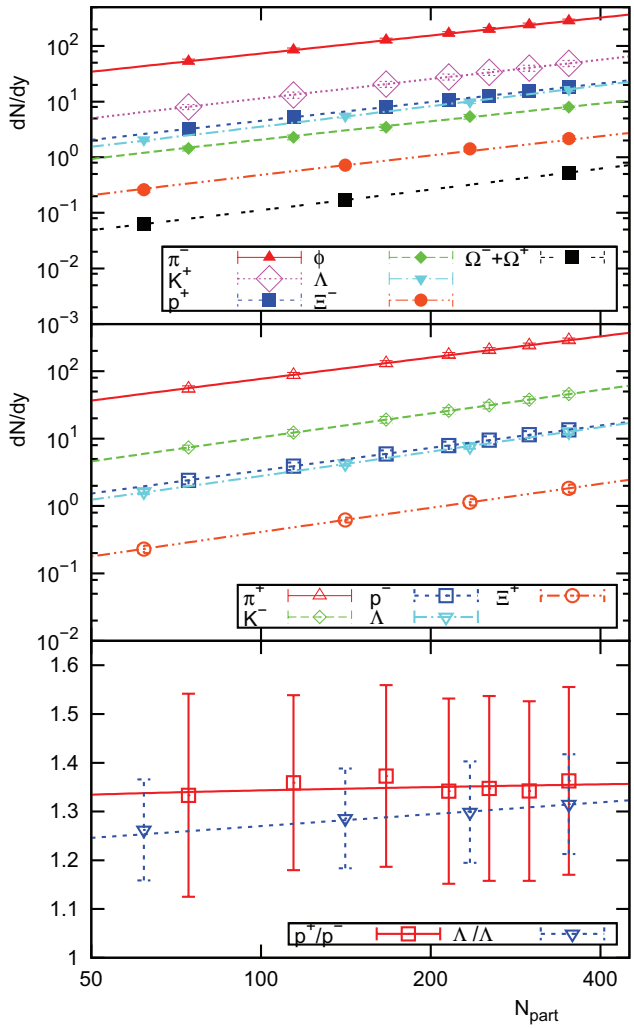

FIG. 4: Fit to particles' yields data at 200 GeV.

TABLE IV: Additional values used to fit each of the centrality bins apart from the particle yields.

$(Q-\overline{Q})/(B-\overline{B})$	0.39 ± 0.01
$(s-\overline{s})/(s+\overline{s})$	0.00 ± 0.05
$P\,[\mathrm{MeV/fm^3}]$	82.0 ± 0.5
$E/h_p\,[\mathrm{MeV}]$	750 ± 2

further, that our approach was consistent on the given interval.

During fitting we discovered that the interpolated proton and antiproton yields do not agree with the model at all. Fitting them or not fitting them does not make the fit converge to a different minimum, it just introduces a large reduction of the statistical significance due to the inability to fit the proton (antiproton) yield. The Λ yield behaves similarly as these two particles are closely bound by the weak decay corrections. In Fig.8 we show the ratio of the data over statistical model prediction for proton

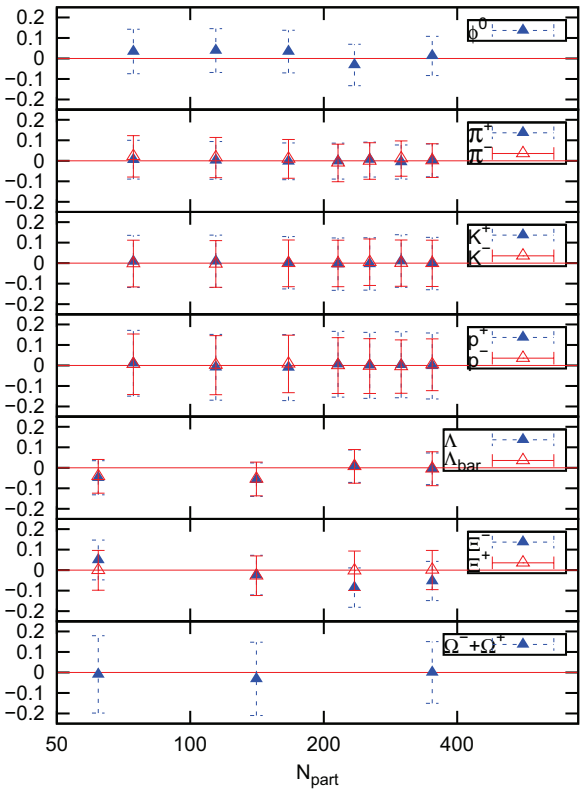

FIG. 5: The difference between experimental values and fitted function with errors all scaled with the theoretically predicted value $((data - fit)/fit \pm error/fit)$ at 200 GeV.

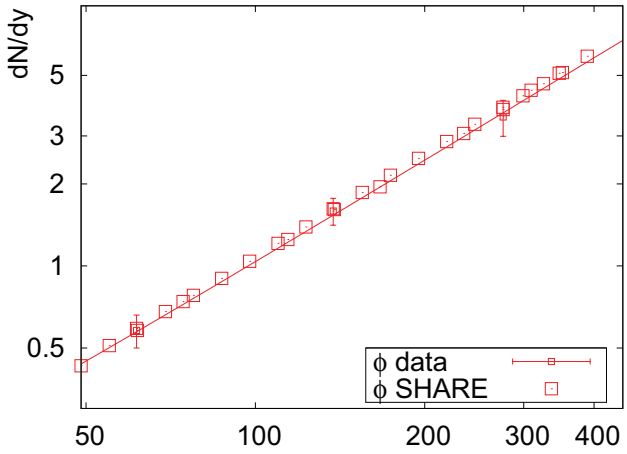

FIG. 6: Fit of ϕ^0 on the background of other particles at 62.4 GeV.

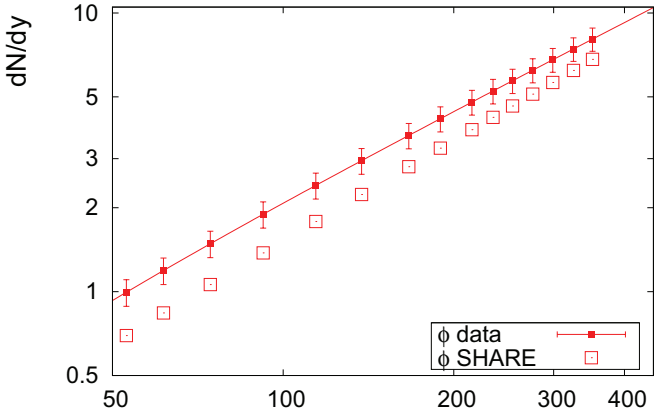

FIG. 7: Fit of ϕ^0 on the background of other particles at 200 GeV.

and lambda yields. It turns out that this ratio is fluctuating around a constant value. We assumed that the normalization of these yields was not correct and therefore tried to fit the particle/antiparticle ratio of protons and Λs respectively, so their absolute yield will not come into the statistical model calculation. We fit the ratios and they are consistent with other particle yields.

IV. RESULTS

Let us discuss first how the particles were fitted. In the following paragraphs we present our findings and discuss each of the results separately. Fit for each centrality bin has been done independently of each other. The only connection between the neighbouring centrality bins is that final parameters of each fit has been given as initial parameters to the following one, going from most central to peripheral bins. Very high confidence level (we distinguish two confidence levels in this article, CL-I – confidence level of the particle interpolation as described in the previous section and CL-S – confidence level of the physical fit with SHARE model), above 96%, has been reached for each of the fits. The final model parameters for can be found in Table.VII.

A. Particle yields

As mentioned in the introduction, we succesfully fit the ϕ yield as one can see on Figure 6. This procedure was done for all the particles and served also as a sanity check of our particle interpolating described in section II. $\pi^{\pm}$,$K^{\pm}$ and $\Xi^{\pm}$ are fitted with comparable precision as the one of ϕ as well as $p^{\pm}$ and Λ ratios for reasons discussed in previous section. We observed that the ratio of experimental value to our model prediction does not change across centrality (Figure 8) and is essentially the same for both particle and antiparticle (2 for protons and roughly 1.4 (or $\sqrt{2}$) for Λs, although the lines in Figure

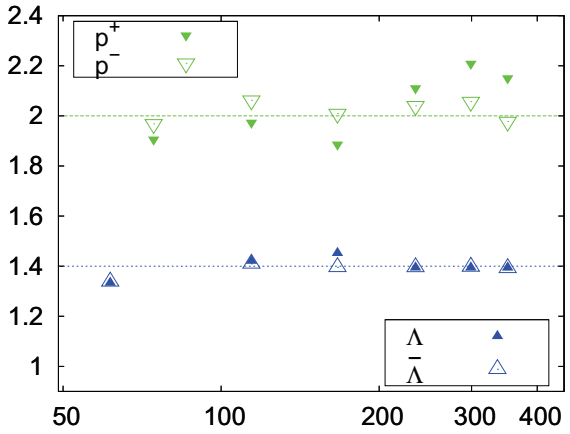

FIG. 8: $p^{\pm}$ and $\Lambda, \overline{\Lambda}$ ratios of experimental data over SHARE yield prediction at 62.4 GeV.

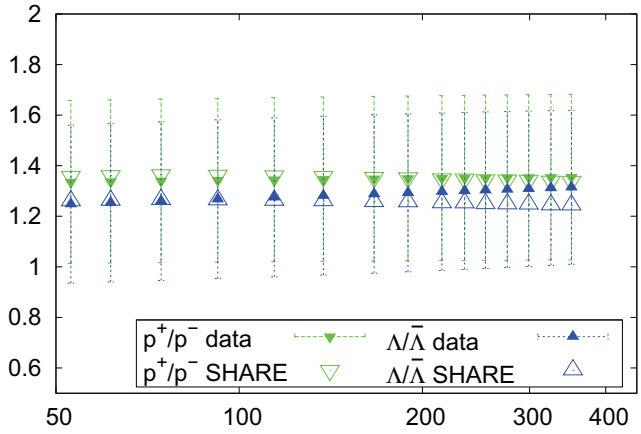

FIG. 9: Ratios of experimental particle over antiparticle data for $p^{\pm}$ and $\Lambda, \overline{\Lambda}$ compared to SHARE ratio prediction at 200 GeV.

8 are only to guide the eye). A slight raise of the proton ratio can be observed in the most central region. We conclude that this proton yield enhancement might be due to counting some of the initial protons coming to the collision. Not to avoid these particles completely, we suggest that the normalization of their respective yields might not be correct. That is why we look at their respective particle to antiparticle ratios (interpolation discussed in Section II) and succesfully fit those.
In the 200 GeV data, switching the ϕ on and off has a dramatic effect on the fit, and reduces confidence levels by as much as 50%. As shown in 7 the ϕ data shows a systematic discrepancy with the fit results. For this reason they are not incuded in our results. The protons and Λs do not produce a different fit, but also somewhat reduce confidence. As in the 62.4 GeV case we fit the particle-antiparticle ratios instead of absolute yields. As shown in 9 the result quite closely matches the experimental data. While as in the 62.4 GeV case we observe a slight increase in proton yield for the most central collisions, we actually see a greater increase in Λ-$\bar{\Lambda}$ ratio.

B. Temperature and chemical potentials

The temperature at kinetic freeze–out of non equilibrium model has the value varying from $T = 139$ MeV for the most central collisions to 141 MeV for the periferal collisions. For the precise evolution see the top left plot of Fig.10. The semi-equilibrium model however, shows temperature varying from $T = 170$ MeV for the peripheral collisions decreasing to about $T = 168$ MeV for the most central collisions. Both models experience a steady decrease of about 2 MeV over the discussed centrality region. One can see that our particle interpolation fits show a high level of consistency going from most central collisions to the peripheral ones.

The baryo-chemical potential μ_B can be seen in the upper right corner of Fig.10. Both of the models show an increase of baryo-chemical potential with number of participants N_{part}. Their values vary from 45 MeV for the non-equilibrium model and 55 MeV for the semi-equilibrium raising to 62 MeV and 77 MeV respectively. Similarly to the temperature, the baryo-chemical potential μ_B shows qualitatively the same behavior, only its values are larger for the semi-equilibrium model.
The strange chemical potential μ_B is increasing with number of participants from 9 MeV (12 MeV) to about 14 MeV (20 MeV) for the non-equilibrium (semi-equilibrium) model respectively as visible in the lower right part of Fig.10.
For both models we observe strangeness enhancement for most central collisions. In the lower left part of Fig.10 we show γ_s/γ_q (γ_s) behavior for the non (semi)-equilibrium model respectively. The evolution of the strange phase space occupancies relative to the non-strange is compatible with the assumption of fast hadronization where the equilibrium in QGP is different from the one of hadron gas and during hadronization some degrees of freedom freeze.
As 11 shows, for the most peripheral collisions the temperature is approximately 141.5 MeV for both 62.4 and 200 GeV. However as the centrality increases, the 62.4 GeV temperature drops under 139 MeV, whereas the 200 GeV temperature is still 140 MeV for the most central collisions. For all centralities and both energies γ_q is essentially constant just under 1.6. These results are consistent with the enhanced pair production shown in Figure **??**. Both the baryo-chemical and strange chemical potentials are lower at 200 GeV than at 62.4 GeV by a factor of two. With increasing centrality the discrepancy in chemical potential only increases. We observe strangness enhancement with centrality at both 62.4 and 200

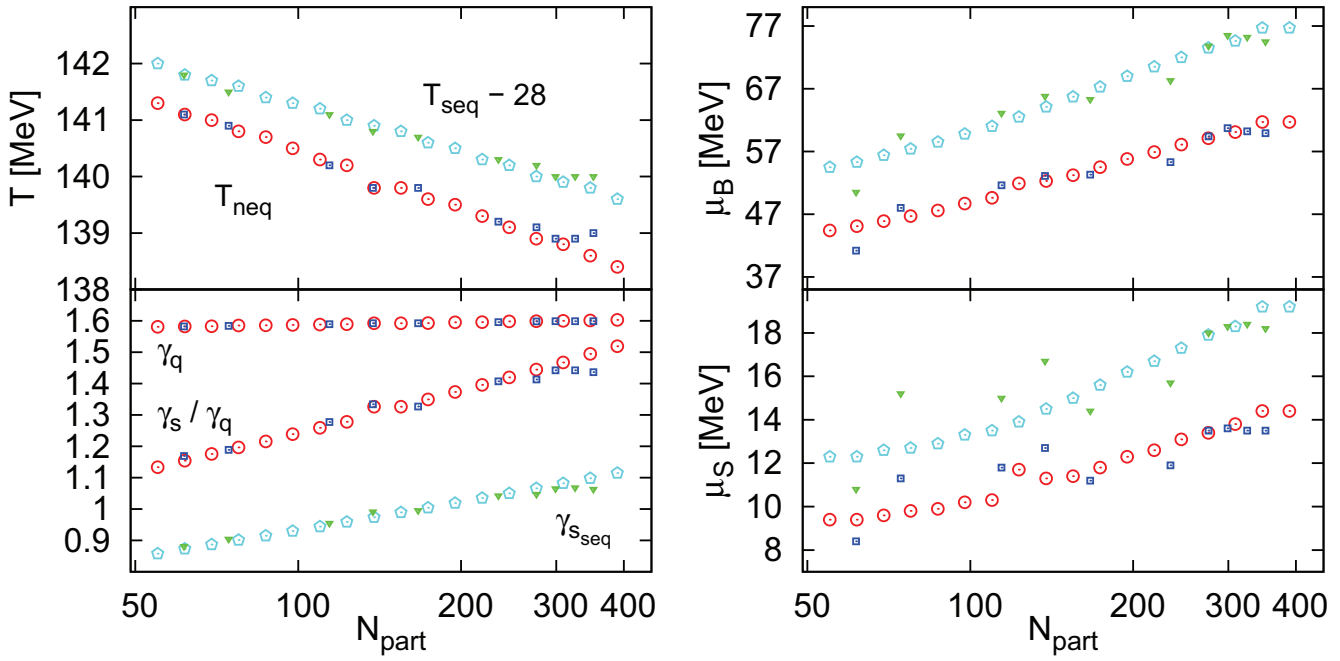

FIG. 10: Statistical parameters and bulk properties of the fireball at the time of kinetic freezeout. Circles present fits with only interpolated values of particle yields, full squares are fits with at least one experimental value (in most cases almost only experimental values, see Table V for details).

GeV, but the latter is not as strong. Again, looking at Figure **??** we expect to see more strangeness at 62.4 GeV. We will discuss this further in Section IV C.

C. System Expansion

We present (Fig.12) the system expansion as a ratio of the volume per unit rapidity resulting from our fit (V) compared to the volume of the colliding participants V_N as calculated using the empirical formula for nuclear radius and assuming a spherical shape of the colliding nuclei.

$$V_N = \Delta y \cdot N_{part} \left(\frac{4\pi}{3}\right) (1.18)^3, \qquad (4)$$

where Δy is the rapidity of the projectile and target. In the case of 62.4 GeV we use the value $\Delta y = 8.48$ and $\Delta y = 10.6$ fot 200 GeV. We observe in Fig.12 that the system expands and the rate of expansion grows from peripheral to central collisions for both non and semi-equilibrium model. The expansion is much more significant at 200 GeV. This is consistent with our results for γ_s discussed above, indicating that the system has not enough time to fully develop strangeness.

D. Hadronization conditions

In the left part of Fig.13 we present how closely our fits follow the hadronization conditions we present in section III. These conditions are met by both models. When we are not fitting pressure for the semi-equilibrium model, it stays constant. We do not fit it to keep the number of degrees of freedom constant, as γ_q is fixed to 1 for the semi-equilibrium model.
The E/TS is above 1 which suggests explosive behavior, unlike the the value for semi-equilibrium. It shows only small variation across centrality.
The ratio of strangeness over entropy s/S can be seen in Figure 14 to increase with number of participants. Both models show comparable behavior as seen in the lower right corner of Fig.13. While they have been separated for clarity, one can see that the energy per primary hadron and pressure are constant at both energies. In our fitting we constrain the energy per primary hadron and the pressure of the system, as discussed in Section III. E/TS increases very slightly with centrality, but is always greater than one, implying explosive behavior. The strangeness over entropy (s/S) is the same across energy for the most peripheral collisions, but as centrality increases the 62.4 GeV data displays a higher ratio. Because entropy appears more quickly than strangeness in the evolution of the fireball, this is indicative of a more rapid hadronization at 200 GeV (see Section IV C).

E. Bulk properties

In the left part of Fig.15 we show the effective number of degrees of freedom g_{eff} (top) and effective number of strange degrees of freedom g^s_{eff} (bottom). Both models

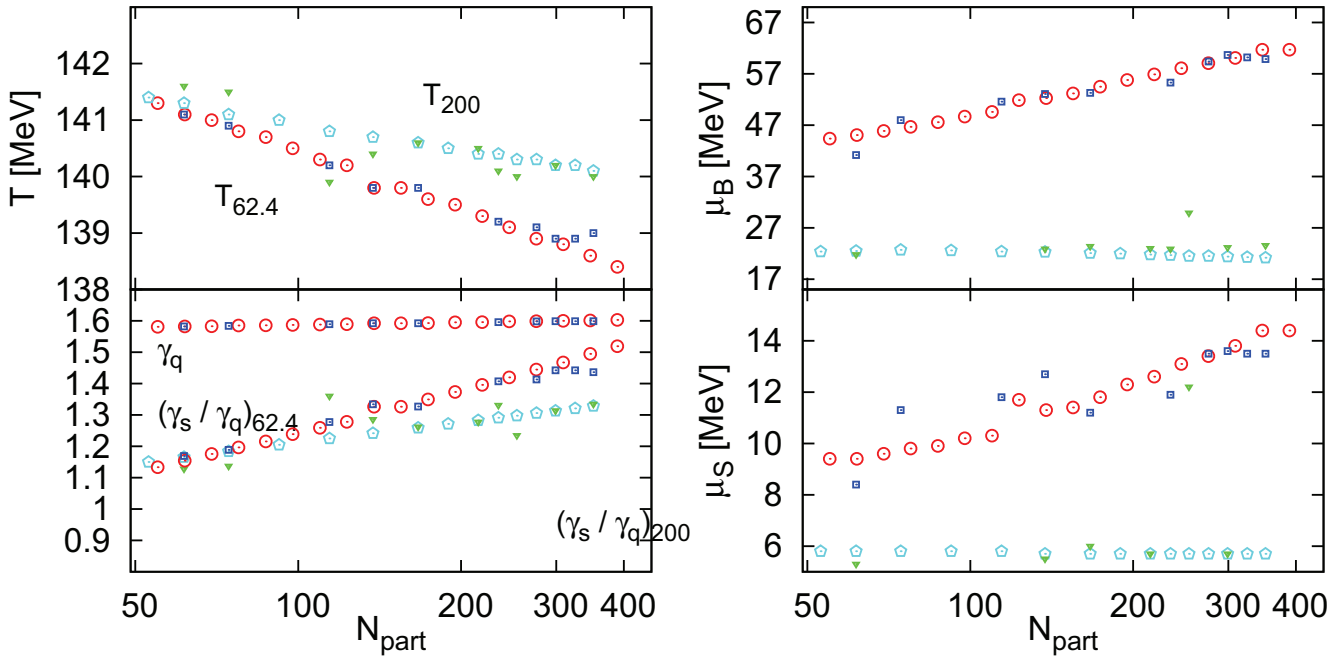

FIG. 11: Statistical parameters and bulk properties of the fireball at the time of kinetic freezeout, compared at 62.4 and 200 GeV. Circles present fits with only interpolated values of particle yields, full squares are fits with at least one experimental value (see Table V for details).

show increase in these quantities going from peripheral to central collisions.

On the right side of Fig.15 we present the entropy density σ and energy density ε. Both are constant across centrality and higher for semi equilibrium model.

The energy and entropy densities shown in Figure 16 appear to remain constant at both energies across centrality, at approximately 485 MeV/fm^3 and 3.36 fm$^-$3 respectively. We see as well that the effective degrees of freedom are the same for 62.4 and 200 GeV. However, the effective number of strange degrees of freedom shows different behavior across energies. As in our previous discussion we see an enhancement of strangeness with centrality, but one that is greater at 62.4 Gev than at 200.

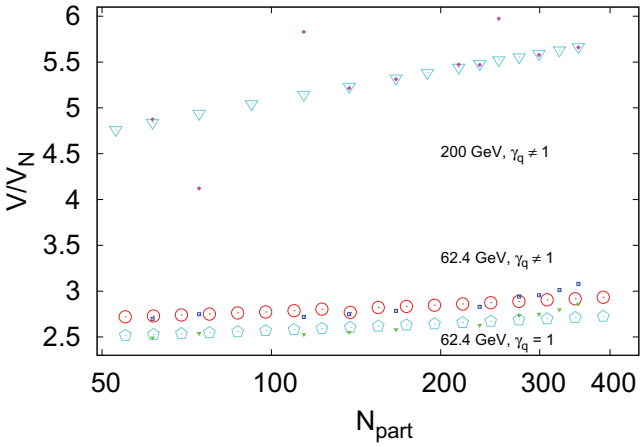

FIG. 12: Volume at hadronization (V) to nuclear volume (V_N) ratio.

V. CONCLUSION

In this work we provide detailed centrality dependence of bulk properties of the fireball in heavy ion collisions in the framework of statistical hadronization model. We tune the model parameters to available data from Au-Au collisionas at $\sqrt{s_{NN}} = 62.4$ GeV and 200 GeV. We emphasize succesful fitting of ϕ on the background of other particles at the lower energy. We compare two models, chemical non-equilibrium and semi-equilibrium and discuss fast hadronization scenario, strangeness enhancement and bulk properties as a function of collision centrality.

VI. ACKNOWLEDGEMENTS

MP and JR: supported by a grant from the U.S. Department of Energy, DE-FG02-04ER41318 . JL: Laboratoire de Physique Théorique et Hautes Energies, LPTHE, at University Paris 6 and 7 is supported by CNRS as Unité Mixte de Recherche, UMR7589. GT: supported by the Helmholtz International Center for FAIR within the framework of the LOEWE program (Landesoffensive zur Entwicklung Wissenschaftlich-ökonomischer Exzel-

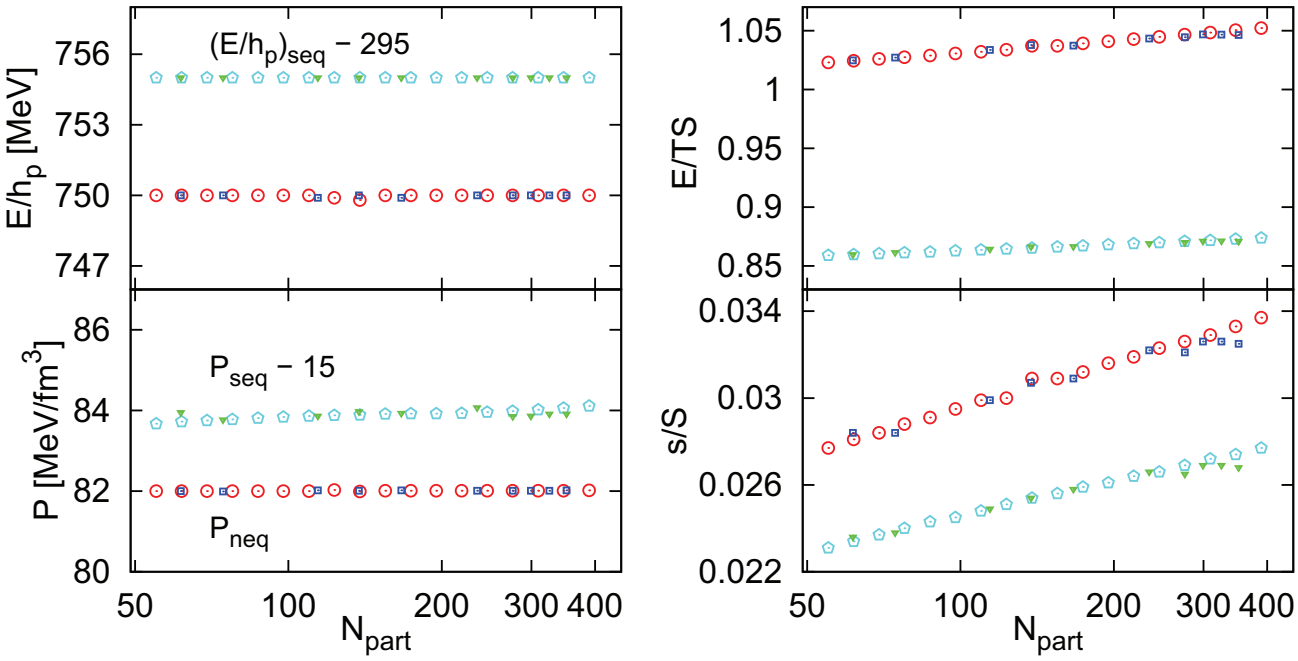

FIG. 13: Bulk properties of the fireball at the time of kinetic freezeout. Symbols chosen accordingly to Figure 10. The left top plot presents pressure P and left bottom one energy per primary hadron E/h_p, which were fitted. The right top plot shows the behavior of E/TS and right bottom strangeness per entropy s/S content.

lenz) by the State of Hesse.

[1] B. I. Abelev *et al.* [STAR Collaboration], [arXiv:nucl-ex/0809.4737v1].
[2] L. Molnár [STAR Collaboration], [arXiv:nucl-ex/0805.3086v2].
[3] J. Speltz [STAR Collaboration] [http://eprints-scd-ulp.u-strasbg.fr:8080/714/].
[4] J. Takahashi, Personal communication.
[5] J. Rafelski, J. Letessier, [arXiv:hep-ph/0901.2406v1].
[6] J. Rafelski, J. Letessier, [arXiv:hep-ph/0902.0063v1].
[7] J. Adams *et al.*, [arXiv:nucl-ex/0511026v1].
[8] C. Amsler *et al.*, Physics Letters **B667**, 1 (2008).
[9] J. Letessier, J. Rafelski, [arXiv:nucl-th/0602047].
[10] G. Torrieri, S. Steinke, W. Broniowski, W. Florkowski, J. Letessier, J. Rafelski, [arXiv:nucl-th/0404083v2].
[11] G. Torrieri, S. Jeon, J. Letessier, J. Rafelski [arXiv:nucl-th/0603026v2].
[12] S. S. Adler *et al.*, [arXiv:nucl-ex/0307022].
[13] J. Adams *et al.*, [arXiv:nucl-ex/0606014].
[14] B.I. Abelev *et al.*, [arXiv:nucl-ex/0809.4737]

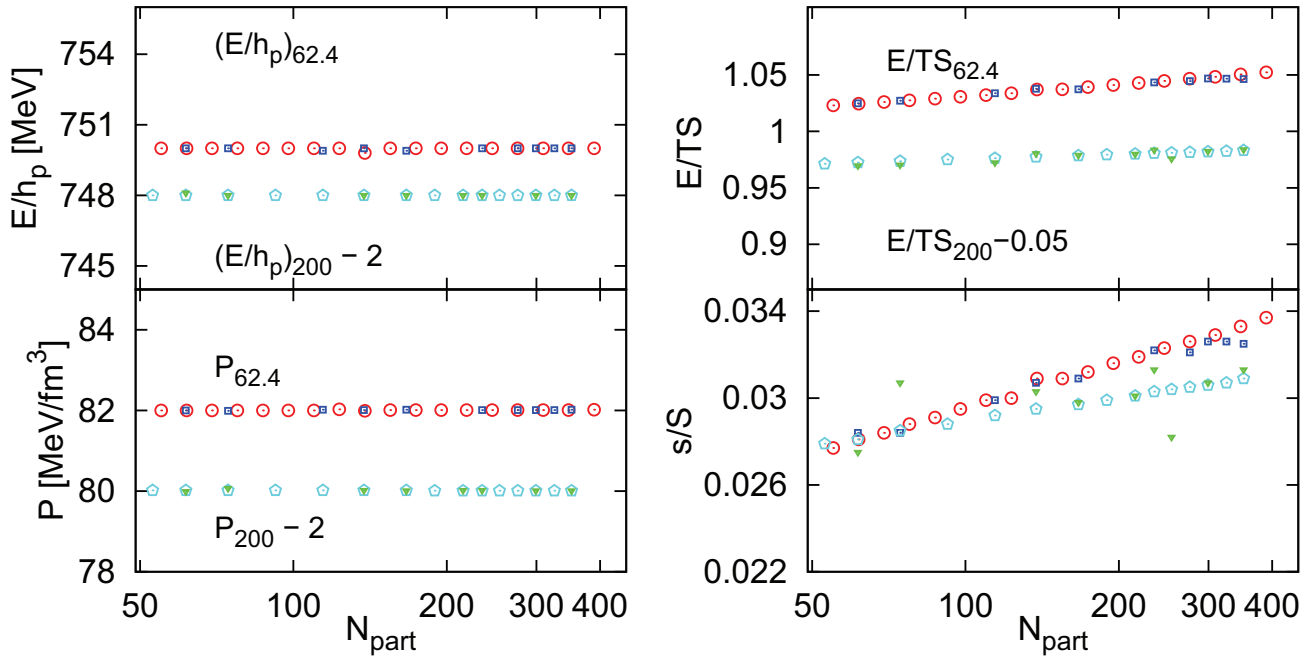

FIG. 14: Bulk properties of the fireball at the time of kinetic freezeout, compared at 62.4 and 200 GeV. Symbols chosen accordingly to Figure 10. The left top plot presents pressure P and left bottom one energy per primary hadron E/h_p, which were fitted. The right top plot shows the behavior of E/TS and right bottom strangeness per entropy s/S content.

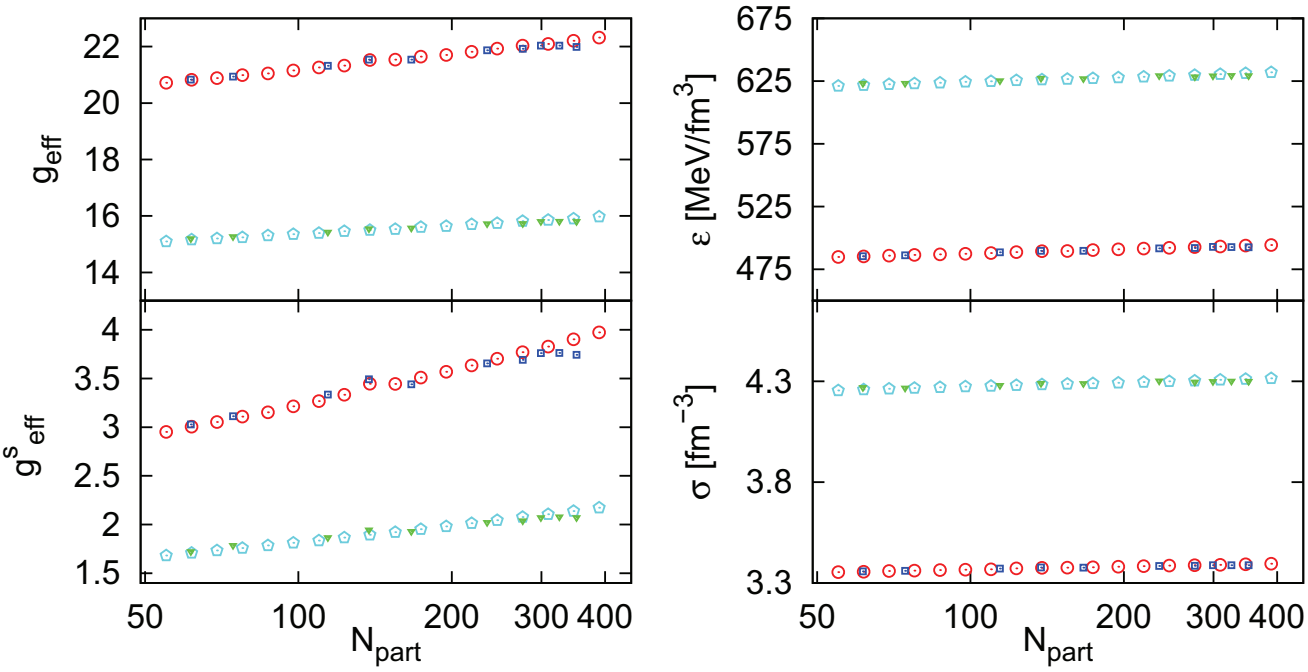

FIG. 15: Right column show the effective number of degrees of freedom (g_{eff}) and the effective number of strange degrees of freedom(g^s_{eff}. The right column shows energy density (ε) and entropy density (σ).

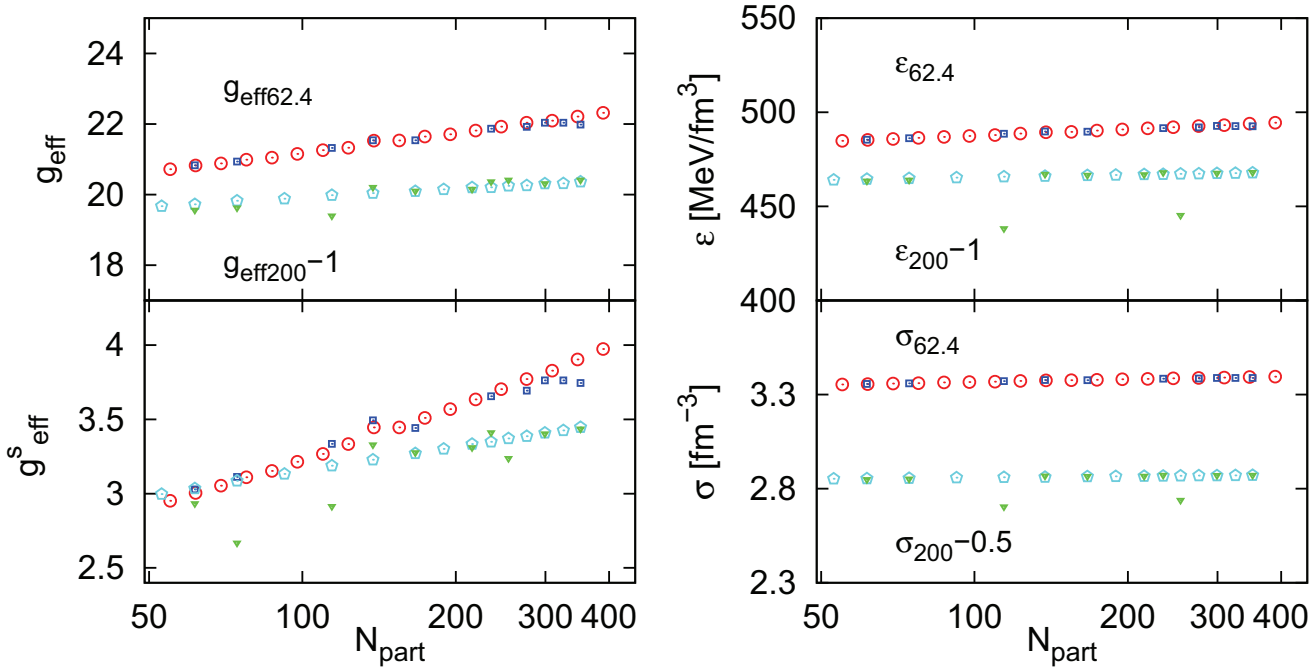

FIG. 16: Comparison of bulk properties at 62.4 and 200 GeV. Right column show the effective number of degrees of freedom (g_{eff}) and the effective number of strange degrees of freedom(g^s_{eff}. The right column shows energy density (ε) and entropy density (σ).

TABLE V: Table of used particle yields at 62.4 GeV. Experimental data are displayed in **bold**.

N_{part}	61.5	74.4	114.2	137.5	166.6
π^-	35.25 ± 3.4	**43.8 ± 3.4**	**67.5 ± 5.5**	82.0 ± 9.0	**101 ± 9.0**
π^+	35.68 ± 3.4	**43.2 ± 3.4**	**66.6 ± 5.4**	82.3 ± 8.5	**98.9 ± 8.5**
K^+	5.18 ± 0.50	**6.58 ± 0.5**	**10.3 ± 0.8**	12.6 ± 1.31	**15.6 ± 1.31**
K^-	4.54 ± 0.43	**5.64 ± 0.43**	**8.78 ± 0.7**	10.9 ± 1.20	**13.7 ± 1.20**
Λ (not fitted)	**1.68 ± 0.04**	2.33 ± 0.08	**3.68 ± 0.08**	4.66 ± 0.09	**5.88 ± 0.09**
$\overline{\Lambda}$ (not fitted)	**1.07 ± 0.02**	1.31 ± 0.04	**2.1 ± 0.04**	2.56 ± 0.05	**3.14 ± 0.05**
Ξ^-	**0.20 ± 0.01**	0.24 ± 0.03	0.43 ± 0.03	**0.55 ± 0.03**	0.69 ± 0.07
$\overline{\Xi}^+$	**0.14 ± 0.01**	0.18 ± 0.02	0.29 ± 0.02	**0.38 ± 0.02**	0.45 ± 0.04
$\Omega + \overline{\Omega}$ (not fitted)	**0.034 ± 0.007**	0.043 ± 0.008	0.076 ± 0.014	**0.100 ± 0.014**	0.13 ± 0.03
p^+ (not fitted)	5.68 ± 0.43	**5.68 ± 0.43**	**8.88 ± 0.7**	11.0 ± 1.10	**12.9 ± 1.10**
p^- (not fitted)	3.05 ± 0.23	**3.05 ± 0.23**	**4.64 ± 0.37**	5.51 ± 0.65	**6.65 ± 0.65**
ϕ^0	**0.58 ± 0.08**	0.77 ± 0.18	1.25 ± 0.18	**1.59 ± 0.18**	1.91 ± 0.53
p^+/p^-	1.79 ± 0.28	**1.86 ± 0.28**	**1.91 ± 0.3**	1.98 ± 0.33	**1.94 ± 0.36**
$\Lambda/\overline{\Lambda}$	**1.57 ± 0.07**	1.67 ± 0.07	**1.75 ± 0.07**	1.77 ± 0.07	**1.81 ± 0.07**
N_{part}	234.6	275.7	299.0	325.2	351.4
π^-	**146 ± 13**	178.9 ± 20	**192 ± 20**	217.9 ± 24	**237 ± 27**
π^+	**144 ± 14**	173.5 ± 20	**191 ± 20**	208.4 ± 23	**233 ± 26**
K^+	**22.9 ± 2.1**	28.14 ± 3.16	**31.2 ± 3.16**	34.4 ± 3.7	**38.0 ± 4.3**
K^-	**19.7 ± 1.8**	24.35 ± 2.80	**27.1 ± 2.8**	29.6 ± 3.3	**32.6 ± 3.7**
Λ (not fitted)	**8.28 ± 0.13**	10.23 ± 0.23	**11.39 ± 0.23**	12.4 ± 0.23	**13.88 ± 0.23**
$\overline{\Lambda}$ (not fitted)	**4.52 ± 0.07**	5.46 ± 0.12	**5.91 ± 0.12**	6.54 ± 0.13	**7.25 ± 0.13**
Ξ^-	1.09 ± 0.07	1.33 ± 0.08	**1.50 ± 0.08**	1.68 ± 0.11	**1.84 ± 0.11**
$\overline{\Xi}^+$	0.69 ± 0.04	0.85 ± 0.06	**0.94 ± 0.06**	1.06 ± 0.08	**1.16 ± 0.08**
$\Omega + \overline{\Omega}$ (not fitted)	0.22 ± 0.03	0.27 ± 0.05	0.31 ± 0.05	**0.35 ± 0.05**	0.41 ± 0.05
p^+ (not fitted)	**20.2 ± 1.9**	24.88 ± 2.9	**28.8 ± 2.9**	34.3 ± 3.8	**34.3 ± 3.8**
p^- (not fitted)	**9.12 ± 0.83**	11.1 ± 1.2	**11.6 ± 1.2**	13.8 ± 1.6	**13.8 ± 1.6**
ϕ^0	2.83 ± 0.53	**3.52 ± 0.53**	3.76 ± 0.65	4.16 ± 0.65	4.57 ± 0.65
p^+/p^-	**2.21 ± 0.41**	2.33 ± 0.46	**2.48 ± 0.51**	2.45 ± 0.54	**2.49 ± 0.56**
$\Lambda/\overline{\Lambda}$	**1.83 ± 0.06**	1.9 ± 0.06	**1.93 ± 0.08**	1.92 ± 0.08	**1.91 ± 0.07**

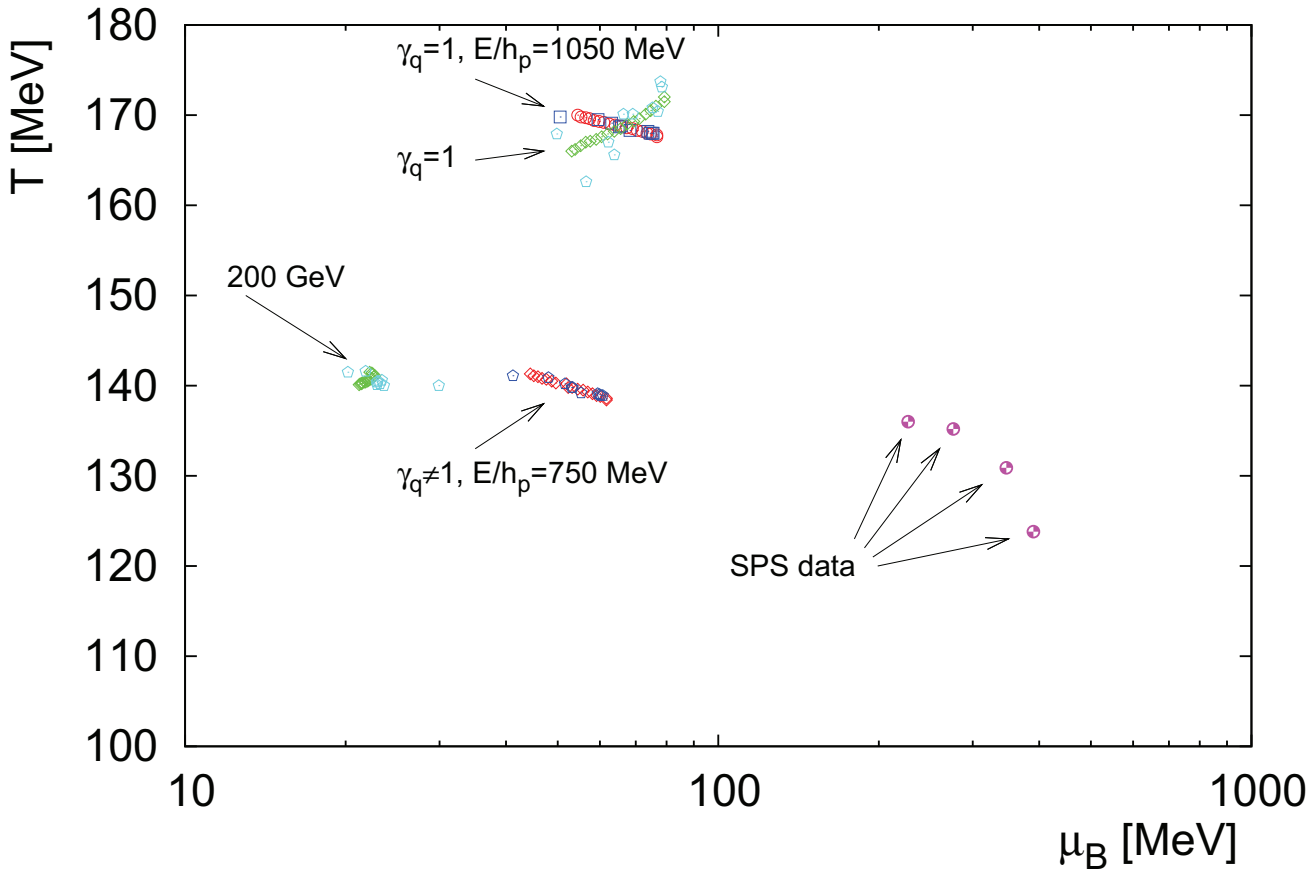

FIG. 17: Temperature as a function of baryo-chemical potential μ_B.

TABLE VI: Table of used particle yields at 200 GeV.

N_{part}	61.5	74.4	114.2	137.5	166.6
π^-	43.221 ± 4.122	53.184 ± 5.037	84.566 ± 7.837	103.288 ± 9.448	126.956 ± 11.423
π^+	45.789 ± 4.662	56.140 ± 5.668	88.430 ± 8.696	107.526 ± 10.409	131.531 ± 12.481
K^+	6.441 ± 0.823	8.067 ± 1.031	13.321 ± 1.702	16.529 ± 2.113	20.645 ± 2.640
K^-	5.887 ± 0.671	7.383 ± 0.842	12.248 ± 1.395	15.235 ± 1.734	19.082 ± 2.171
Λ (not fitted)	1.974 ± 0.164	2.479 ± 0.206	4.165 ± 0.342	5.226 ± 0.427	6.614 ± 0.536
$\overline{\Lambda}$ (not fitted)	1.575 ± 0.130	1.968 ± 0.162	3.268 ± 0.269	4.079 ± 0.336	5.135 ± 0.423
Ξ^-	0.268 ± 0.026	0.337 ± 0.033	0.561 ± 0.054	0.697 ± 0.067	0.871 ± 0.084
$\overline{\Xi}^+$	0.230 ± 0.022	0.289 ± 0.028	0.484 ± 0.047	0.603 ± 0.058	0.758 ± 0.073
$\Omega + \overline{\Omega}$ (not fitted)	0.062 ± 0.012	0.078 ± 0.015	0.131 ± 0.024	0.165 ± 0.029	0.209 ± 0.037
p^+ (not fitted)	2.602 ± 0.418	3.235 ± 0.520	5.253 ± 0.845	6.470 ± 1.041	8.017 ± 1.291
p^- (not fitted)	1.945 ± 0.289	2.414 ± 0.356	3.907 ± 0.565	4.804 ± 0.686	5.946 ± 0.836
ϕ^0	1.190 ± 0.130	1.485 ± 0.161	2.406 ± 0.257	2.950 ± 0.312	3.634 ± 0.379
N_{part}	234.6	275.7	299.0	325.2	351.4
π^-	183.244 ± 15.848	217.803 ± 18.378	237.546 ± 19.759	259.864 ± 21.266	282.297 ± 22.722
π^+	188.156 ± 17.012	222.670 ± 19.530	242.317 ± 20.882	264.472 ± 22.335	286.688 ± 23.717
K^+	30.649 ± 3.921	36.910 ± 4.724	40.521 ± 5.187	44.630 ± 5.715	48.786 ± 6.248
K^-	28.481 ± 3.235	34.391 ± 3.902	37.807 ± 4.288	41.700 ± 4.726	45.645 ± 5.170
Λ (not fitted)	10.081 ± 0.803	12.305 ± 0.969	13.603 ± 1.065	15.093 ± 1.173	16.612 ± 1.283
$\overline{\Lambda}$ (not fitted)	7.754 ± 0.640	9.424 ± 0.779	10.395 ± 0.859	11.508 ± 0.952	12.640 ± 1.046
Ξ^-	1.293 ± 0.124	1.556 ± 0.149	1.708 ± 0.164	1.880 ± 0.180	2.054 ± 0.196
$\overline{\Xi}^+$	1.137 ± 0.109	1.376 ± 0.132	1.514 ± 0.145	1.671 ± 1.160	1.831 ± 1.160
$\Omega + \overline{\Omega}$ (not fitted)	0.320 ± 0.053	0.391 ± 0.063	0.433 ± 0.068	0.481 ± 0.160	0.530 ± 0.175
p^+ (not fitted)	11.732 ± 1.890	14.032 ± 2.261	15.351 ± 2.473	16.847 ± 2.715	18.355 ± 2.958
p^- (not fitted)	8.681 ± 1.175	10.373 ± 1.372	11.342 ± 1.480	12.441 ± 1.598	13.548 ± 1.714
ϕ^0	5.248 ± 0.531	6.232 ± 0.618	6.793 ± 0.666	7.424 ± 0.719	8.058 ± 0.771

TABLE VII: Final statistical parameters for non-equilibrium (upper half) and semi-equilibrium (lower half) fit at 62.4 GeV

N_{part}	$dV/dy\,[fm^3]$	T [MeV]	$\mu_B\,[MeV]$	$\mu_S\,[MeV]$	γ_s	γ_q
351.4	885.61	139.0	59.9	13.5	2.297	1.599
325.2	801.54	138.9	60.2	13.5	2.306	1.599
299.0	723.21	138.9	60.7	13.6	2.306	1.599
275.7	663.73	139.1	59.4	13.5	2.258	1.598
234.6	543.18	139.2	55.3	11.9	2.246	1.596
166.6	379.77	139.8	53.3	11.2	2.112	1.592
137.5	309.37	139.8	53.1	12.7	2.123	1.592
114.2	254.12	140.2	51.6	11.8	2.030	1.589
74.4	167.35	140.9	48.0	11.3	1.883	1.584
61.5	135.82	141.1	41.2	8.4	1.849	1.582
351.4	822.42	168.0	74.5	18.2	1.063	1
325.2	744.81	168.0	75.2	18.4	1.068	1
299.0	673.19	168.0	75.5	18.3	1.065	1
275.7	617.34	168.2	73.8	18.0	1.047	1
234.6	504.42	168.3	68.3	15.7	1.042	1
166.6	352.01	168.7	65.3	14.4	0.995	1
137.5	287.1	168.8	65.8	16.7	0.991	1
114.2	236.16	169.1	63.1	15.0	0.955	1
74.4	154.66	169.5	59.5	15.2	0.904	1
61.5	125.4	169.8	50.5	10.8	0.881	1